

# Synthesis and photocatalytic property of SnO<sub>2</sub>/TiO<sub>2</sub> nanotubes composites

Lin-Rui Hou, Chang-Zhou Yuan, Yang Peng\*

*Institute of Applied Chemistry, Xinjiang University, Urumqi 830046, PR China*

Received 15 February 2006; received in revised form 11 June 2006; accepted 12 June 2006

Available online 16 June 2006

## Abstract

SnO<sub>2</sub>/TiO<sub>2</sub> nanotubes composite photocatalysts with different SnO<sub>2</sub> contents were successfully synthesized by means of a simple solvothermal process. The synthesized products were characterized physically by X-ray diffraction (XRD) and high-resolution transmission electron microscope (HRTEM). The composite photocatalysts can not only make the target pollutant, methylene blue (MB), adsorbed at a high concentration level around the surface of the composites but also decrease the recombination rate of electron–hole pairs so as to achieve good photocatalytic performance. The effect of SnO<sub>2</sub> contents on the photocatalytic activities of the composites was also investigated. The results showed that the SnO<sub>2</sub>/TiO<sub>2</sub> nanotubes composite photocatalyst with 5 wt.% SnO<sub>2</sub> loading had the highest photocatalytic efficiency.

© 2006 Elsevier B.V. All rights reserved.

**Keywords:** SnO<sub>2</sub>/TiO<sub>2</sub> nanotubes composites; Photocatalytic reaction; Methylene blue

## 1. Introduction

Photocatalytically decomposing organic pollutants utilizing an oxide semiconductor to generate clean environment has been a dream of humankind for several decades [1,2]. Particularly, TiO<sub>2</sub> having a crystal form of anatase is known to be one of the most effective photocatalysts for the treatment of polluted water, and its photocatalytic behavior has been studied extensively [3,4]. However, the large band gap in TiO<sub>2</sub> and high recombination rate of the photogenerated electron/hole pairs hinder its further application in industry. To solve these problems, numerous efforts have been attempted to improve its photocatalytic activity by modifying the surface or bulk properties of TiO<sub>2</sub>, such as doping, codeposition of metals, surface chelation, mixing of two semiconductors, etc. [5–7].

Among the coupled semiconductor photocatalysts, many efforts have been devoted to the SnO<sub>2</sub>/TiO<sub>2</sub> system [8,9]. The relatively high photocatalytic activity of SnO<sub>2</sub>/TiO<sub>2</sub> coupled oxide should be attributed to better charge separation. It is well known that the proper placement of the individual semi-

conductor is essential for the charge separation to ensure high photocatalytic activity due to fast electron transfer from TiO<sub>2</sub> to SnO<sub>2</sub>. The bandgaps of SnO<sub>2</sub> and TiO<sub>2</sub> are 3.8 and 3.2 eV, respectively [8]. When the two semiconductor particles are coupled, the conduction band (CB) of SnO<sub>2</sub> ( $E_{CB}$  for SnO<sub>2</sub> = 0 V versus NHE at pH 7) is lower than that of the TiO<sub>2</sub> ( $E_{CB}$  for TiO<sub>2</sub> = –0.5 V versus NHE at pH 7), the former acts as a sink for photogenerated electrons. Since the photogenerated holes move in the opposite direction, they accumulate in the valence band of the TiO<sub>2</sub> particles, thereby increasing the efficiency of charge separation [9].

It has been reported that TiO<sub>2</sub> with higher specific surface area demonstrated a better photocatalytic performance than the simple TiO<sub>2</sub> particles [10]. Therefore, it is of great interest to find a special technique that enables the photocatalyst with higher specific surface area to decompose pollutants with high reaction rate and may be easily applied to industry. TiO<sub>2</sub> nanotubes have been found to give some advantages for TiO<sub>2</sub> nanoparticles because of their larger specific area surface [11]. TiO<sub>2</sub> nanotubes make a high concentration environment of target pollutants around photocatalysts, hence, increasing the collision probability between pollutants and photocatalysts [11,12].

In this study, we prepared the SnO<sub>2</sub>/TiO<sub>2</sub> nanotubes composite photocatalysts that offer considerably higher photocatalytic

\* Corresponding author.

E-mail address: ym0808@sohu.com (Y. Peng).

efficiency than that of pure TiO<sub>2</sub> nanotubes toward the oxidation of methylene blue in aqueous solution. The influence of the SnO<sub>2</sub> contents on the photocatalytic activity of the composite photocatalysts was investigated.

## 2. Experimental

### 2.1. Synthesis of the SnO<sub>2</sub>/TiO<sub>2</sub> nanotubes composite photocatalysts

All chemicals were of analytical grade and used without further purification. The method employed for the synthesis of TiO<sub>2</sub> nanotubes was the same as described in Refs. [11–13], except where otherwise indicated. The distilled deionized water was used for preparing solutions. In the classical synthesis, 0.8 g pure TiO<sub>2</sub> powders of anatase phase were mixed with 10 M KOH aqueous solution in a Teflon-lined autoclave at 200 °C for 24 h. The resulted product was treated with 0.1 M HCl and further washed with distilled water and ethanol until the pH reached around 7. The snow-white sample was dried at 78 °C for 7 h.

SnO<sub>2</sub>/TiO<sub>2</sub> nanotubes composite photocatalysts were synthesized by means of the solvothermal method as follows: certain amount of SnCl<sub>4</sub>·5H<sub>2</sub>O was dissolved in absolute ethanol and agitated at room temperature for 30 min to form the well-proportioned solution and then the proper TiO<sub>2</sub> nanotubes were dispersed in the above solution, stirred for 15 min and then ultrasonically treated for 10 min. After well mixed, the mixture was kept in a Teflon-lined autoclave with a stainless steel shell. This autoclave was heated to 160 °C at 10 °C/min in an oven. The autoclave was cooled to room temperature naturally after keeping at 160 °C for 16 h. The prepared products were filtered, washed repeatedly with distilled water and ethanol, and then dried at 80 °C. By changing the added amount of TiO<sub>2</sub> nanotubes to synthesize the SnO<sub>2</sub>/TiO<sub>2</sub> nanotubes composites with 2, 5, 10, 15 wt.% SnO<sub>2</sub> loadings, labeled by S<sub>2</sub>T, S<sub>5</sub>T, S<sub>10</sub>T, S<sub>15</sub>T, respectively, while pure TiO<sub>2</sub> nanotubes are labeled by S<sub>0</sub>T.

### 2.2. Characterization of the SnO<sub>2</sub>/TiO<sub>2</sub> nanotubes composite photocatalysts

The prepared SnO<sub>2</sub>/TiO<sub>2</sub> nanotubes composite photocatalysts were characterized by X-ray diffraction (XRD, Max 18<sup>XCE</sup>, Japan) using a Cu Kα source (λ = 0.154056 nm), scanning electronic microscope (SEM, LEO1430VP, Germany) and high-resolution transmission electron microscope (HRTEM, JEOL 2010 F). The Brunauer–Emmett–Teller (BET) surface area (S<sub>BET</sub>) of the samples was obtained from nitrogen adsorption–desorption data (Micromeritics, ASAP-2010, America). To investigate the light absorption properties of photocatalysts, UV–vis diffuse reflectance spectra were carried out, in the wavelength range of 200–800 nm, using a U-3010 spectrophotometer (Japan). The pure powdered Al<sub>2</sub>O<sub>3</sub> was used as a reference sample.

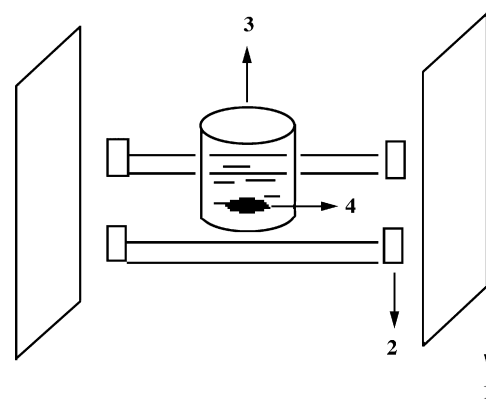


Fig. 1. Photocatalytic reactor. (1) Aluminium reflector, (2) quartz UV lamps (30 W), (3) quartz reactor and (4) magneton.

### 2.3. Adsorption behavior of MB on the synthesized photocatalysts

To determine the adsorption behavior of MB on the synthesized photocatalysts, the suspensions were prepared by mixing 10 ml aliquots of MB solutions of the same initial concentrations ( $5 \times 10^{-5}$  mol/l) with given weight (0.050 g) of different photocatalysts. The suspensions were kept overnight in the dark and filtered after being centrifuged. The absorbance of the filtrate was then measured at the maximum band 464 nm of MB to determine the concentration of MB. The extent of equilibrium adsorption was determined from the decrease in the MB concentration detected after filtration.

### 2.4. Photocatalytic activity measurements

The photocatalytic properties of SnO<sub>2</sub>/TiO<sub>2</sub> nanotubes composite photocatalysts were evaluated by photo-degradation of MB aqueous solution. All photocatalytic reactions were performed under ultraviolet irradiation by using two 30 W ultraviolet lamps and maintaining constant magnetic stirring, and 100 ml of MB solution with initial concentration of  $5 \times 10^{-5}$  mol/l was mixed with 0.050 g as-prepared photocatalyst in a quartz reactor (Fig. 1). The solution was stirred for 10 min in dark to allow the system to reach an adsorption/desorption equilibrium, then analytical samples were drawn from the reaction suspensions every 5 min during the whole irradiation. The concentrations of MB solution were analyzed by UV–vis spectrophotometer (UV-2450, Japan and absorption at λ<sub>max</sub> = 664 nm for MB).

## 3. Results and discussion

### 3.1. XRD analysis

The XRD patterns of the prepared photocatalysts are shown in Fig. 2. As shown in Fig. 2(b)–(e), besides the TiO<sub>2</sub> nanotubes diffraction peaks, there exist the tetragonal SnO<sub>2</sub> diffraction peaks, which are presented and indexed in line with the standard spectrum (JCPDS, No.77-0452). Compared to SnO<sub>2</sub>/TiO<sub>2</sub> nanotubes composites, the peak intensities of pure TiO<sub>2</sub> nanotubes are much stronger than those of SnO<sub>2</sub>/TiO<sub>2</sub> nanotubes

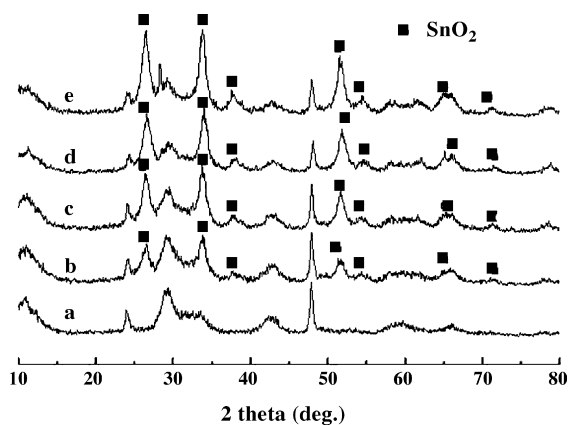


Fig. 2. XRD patterns of S<sub>0</sub>T (a), S<sub>2</sub>T (b), S<sub>5</sub>T (c), S<sub>10</sub>T (d) and S<sub>15</sub>T (e).

composites, which indicate that TiO<sub>2</sub> nanotubes have been successfully coated with the SnO<sub>2</sub> and thus the weakened peaks occurred. Moreover, with the increase of the SnO<sub>2</sub> contents, the peak intensities of SnO<sub>2</sub> become stronger and stronger, while the peak intensities of TiO<sub>2</sub> nanotubes turn weaker and weaker.

### 3.2. The morphology and surface area of samples

#### 3.2.1. The morphology of S<sub>0</sub>T

Fig. 3(a) and (b) shows the SEM and HRTEM images of the as-prepared TiO<sub>2</sub> nanotubes, respectively. The external tube

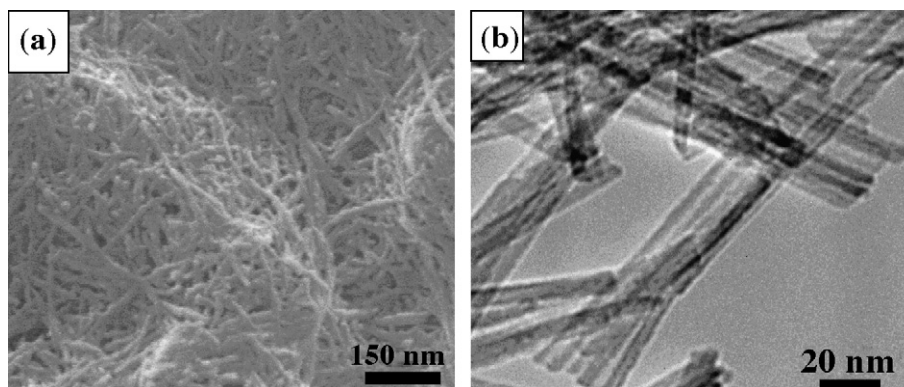


Fig. 3. SEM (a) and HRTEM (b) images of S<sub>0</sub>T.

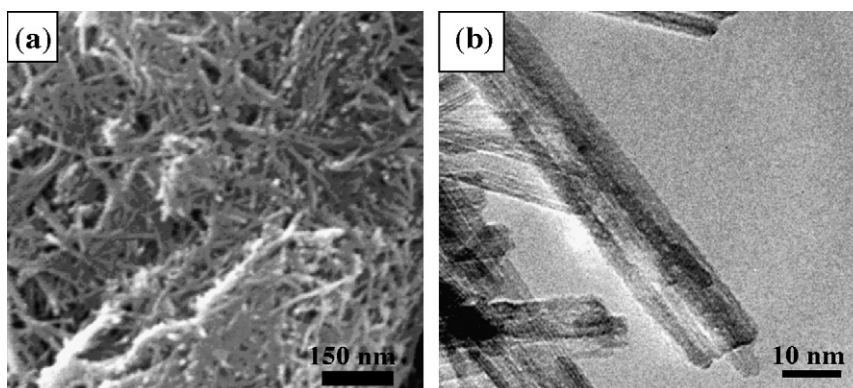


Fig. 4. SEM (a) and HRTEM (b) images of S<sub>5</sub>T.

Table 1  
Surface area for various photocatalysts

	S <sub>BET</sub> (m <sup>2</sup> /g)
S <sub>0</sub> T	280.4
S <sub>2</sub> T	245.9
S <sub>5</sub> T	229.6
S <sub>10</sub> T	211.3
S <sub>15</sub> T	187.8

diameters fall between 10 and 15 nm and the internal diameters are between 7 and 11 nm. The lengths of nanotubes range from 1 to 2 μm. From Fig. 3(b), it can be clearly seen that the nanotubes possess a hollow inner pore with open tube ends.

#### 3.2.2. The morphology of S<sub>5</sub>T

Fig. 4(a) shows the SEM image of the as-prepared S<sub>5</sub>T. As seen in Fig. 4(a), the composites also have nanotube structure, which is provided by the TiO<sub>2</sub> nanotubes. HRTEM study of S<sub>5</sub>T (Fig. 4(b)) reveals that the nanotubes get decorated with evenly distributed SnO<sub>2</sub> nanoparticles without suffering any morphological changes and the thickness of SnO<sub>2</sub> layer is about 1 nm.

#### 3.2.3. The surface areas of as-prepared samples

The surface areas of all photocatalysts in this research are also listed in Table 1. It can be seen that the surface area of pure TiO<sub>2</sub> nanotubes is 280.4 m<sup>2</sup>/g. Moreover, the surface areas of the coupled photocatalysts decreased with the increase of

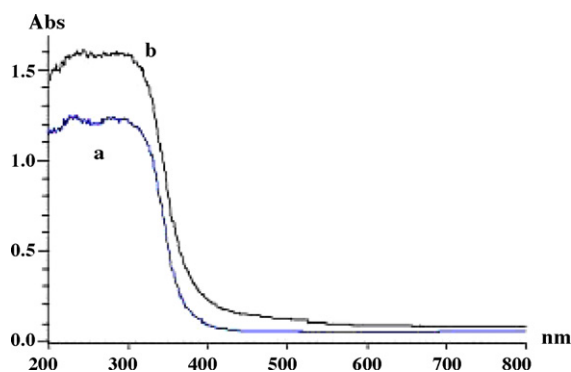


Fig. 5. UV-vis diffuse reflectance spectra of  $S_0T$  (a) and  $S_5T$  (b).

$SnO_2$  contents, indicating that  $SnO_2$  coverage of  $TiO_2$  nanotubes becomes higher while the amount of  $SnO_2$  loadings increases. The increased  $SnO_2$  coverage results in greatly reducing original surface areas and micropore volume of  $TiO_2$  nanotubes. However, the photocatalyst  $S_{15}T$  with a maximum content of  $SnO_2$  still has the  $S_{BET}$  of  $187.8\text{ m}^2/\text{g}$ . For the photocatalytic degradation of dilute pollutants, exposed  $TiO_2$  nanotubes surfaces will service as centers of condensing substrates with a physical adsorption process, and the condensed substrates would be degraded by generated hydroxyl radical.

### 3.3. UV-vis diffuse reflectance spectra analysis

The room temperature UV-vis diffuse reflectance spectra of  $S_0T$  and  $S_5T$  were displayed in Fig. 5. Compared to  $S_0T$ ,  $S_5T$  showed much stronger light absorption property in the UV region and further slightly red-shifted to the visible-light region, which further confirms that  $S_5T$  owned stronger photocatalytic property than  $S_0T$  under UV irradiation. It is known that the process for photocatalysis of semiconductors is the direct absorption of photo by band gap of the material and generates electron-hole pairs in the semiconductor particles. The excitation of an electron from the valence band to conduction band is initiated by light absorption with energy equal to or greater than the band gap of the semiconductor. The narrower band gap is, the more easily an electron is excited from the valence band to the conduction band. The differences in the band gap and light absorption property lead to different photocatalytic behavior. The UV-vis diffuse reflectance spectra are in good agreement with the observed photocatalytic activity.

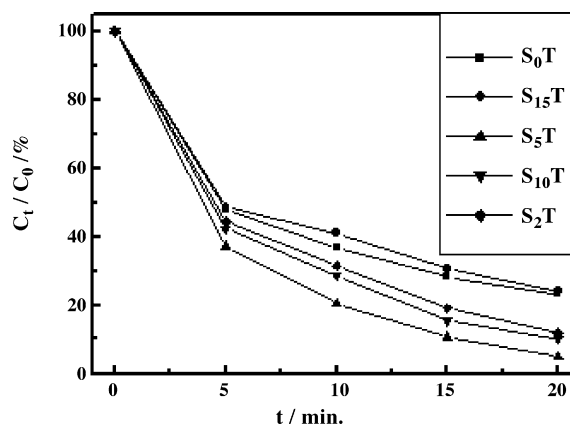


Fig. 6. Effect of as-prepared photocatalysts on the removal efficiency of MB.

### 3.4. Photo-catalytic activity

A preliminary test was done to obtain a few sets of stand control data. The preliminary test was carried out in the dark using the prepared photocatalyst. The results are listed in Table 2. It can be seen that total removal of the model pollutant were not contributed by the effect of photocatalytic degradation alone. A portion of the removal efficiency was attributable to the rapid attainment of adsorption equilibrium of the dye onto the composites, and the  $S_0T$  photocatalyst had the highest adsorption property (25.7%). However, when the photocatalytic degradation experiments were carried out under illumination of light, total removal of pollutant was enhanced significantly. Total removal of pollutant can be attributed to more than 50% of photodegradation capability in addition to the above-mentioned surface adsorption effect.

Removal efficiency of MB over the  $SnO_2/TiO_2$  nanotubes composites with different  $SnO_2$  contents is reported in Fig. 6. It can be seen that  $S_2T$  displayed higher photocatalytic activity compared to  $S_0T$ , and the photocatalytic activity of the  $SnO_2/TiO_2$  nanotubes composite photocatalysts increased with the increase of the  $SnO_2$  content and then decreased slightly. The optimum  $SnO_2$  content was found to be 5 wt.%. Moreover, the photocatalytic activity of  $S_{15}T$  was slower than  $S_0T$ . This indicated that  $SnO_2$  itself was not effective as photocatalyst, which was in agreement with the previous report that  $TiO_2$  nanotubes showed higher photocatalytic property while pure  $SnO_2$  showed very slow photocatalytic activity [11,14,15]. The high photocatalytic activity of the  $SnO_2/TiO_2$  nanotubes composites is attributed to the following two factors: the one is that

Table 2  
Preliminary test and experiments carried out applying optimum parameters

	$S_0T$	$S_2T$	$S_5T$	$S_{10}T$	$S_{15}T$
Initial concentration ( $10^{-5}$ mol/l)	5	5	5	5	5
Adsorption removal <sup>a</sup> ( $10^{-5}$ mol/l/%)	1.285/25.7	1.265/25.3	1.160/23.2	1.080/21.6	0.960/19.2
Photodegradation removal <sup>b</sup> ( $10^{-5}$ mol/l/%)	2.555/51.1	3.150/63.0	3.595/71.9	3.415/68.3	2.845/56.9
Total removal <sup>c</sup> ( $10^{-5}$ mol/l/%)	3.840/76.8	4.415/88.3	4.755/95.1	4.495/89.9	3.805/76.1

<sup>a</sup> Total removal in the dark using photocatalyst.

<sup>b</sup> Total removal – adsorption removal = photodegradation removal.

<sup>c</sup> Total removal under light illumination using photocatalyst.



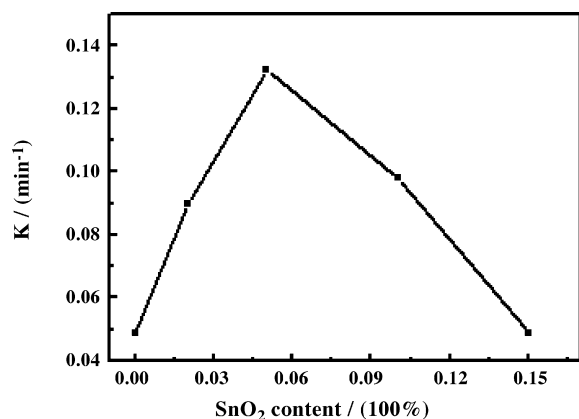


Fig. 7. The photocatalytic activity as a function of the SnO<sub>2</sub> contents for the SnO<sub>2</sub>/TiO<sub>2</sub> nanotubes composite photocatalysts. (photocatalytic reaction rate constants ( $K$ ) were calculated according to the formula:  $\ln(C_0/C_t) = Kt$ , where  $C_0$  and  $C_t$  are the concentrations of MB in the primary stage of experiment and after  $t$  minutes UV-irradiation).

TiO<sub>2</sub> nanotubes make the target pollutants at a high concentration level around the surface of the composite photocatalysts because of their strong adsorption properties, thus the collision rate between pollutants and photocatalysts is increased; the other is the suppression of the recombination rate of the photogenerated electron–hole pairs due to the existence of SnO<sub>2</sub>. Both of the two factors cooperate and make the composite photocatalysts own good photocatalytic performance.

When the SnO<sub>2</sub> content is loaded up to a certain level, such as 15 wt.% SnO<sub>2</sub> loading, a great number of SnO<sub>2</sub> cover the surface of TiO<sub>2</sub> nanotubes, hence decrease the adsorption property of TiO<sub>2</sub> nanotubes, and therefore, the concentration of the target pollutants around of TiO<sub>2</sub> nanotubes is lowered, thus the collision rate between pollutants and photocatalysts is decreased. Moreover, when the loading of SnO<sub>2</sub> is beyond monolayer coverage, the distance of TiO<sub>2</sub> nanotubes from surface of catalyst will increase, so hole and electron cannot be separated effectively. Therefore, the photocatalytic activity of SnO<sub>2</sub>/TiO<sub>2</sub> nanotubes will decrease with the increase of SnO<sub>2</sub> contents when the SnO<sub>2</sub> content is loaded up to a certain level.

Fig. 7 shows the effect of the amount of SnO<sub>2</sub> on the photocatalysts on the kinetic constant  $K$ . It is obvious that  $K$  increases with an increase of SnO<sub>2</sub> contents and the total amount of the SnO<sub>2</sub> is up to ca. 5 wt.%, beyond which a decreasing tendency appears. Therefore, the SnO<sub>2</sub> content should be an important factor affecting the photocatalytic activities of the SnO<sub>2</sub>/TiO<sub>2</sub> nanotubes composite photocatalysts, which is in well agreement with the Ref. [15].

In order to further get some information about the degradation mechanism of MB over the composites, we designed the schematic diagram of the charge-transfer process in the SnO<sub>2</sub>/TiO<sub>2</sub> nanotubes composite photocatalysts, as shown in Fig. 8. When proper SnO<sub>2</sub> is loaded on TiO<sub>2</sub> nanotubes, during the photocatalytic process, the absorption of a photon by TiO<sub>2</sub> nanotubes leads the promotion of an electron from the valence band to the conduction band of TiO<sub>2</sub> nanotubes ( $E_{CB}$  for SnO<sub>2</sub> = 0 V versus NHE at pH 7), and then the electron is transferred to the conduction of SnO<sub>2</sub> ( $E_{CB} = -0.5$  V versus

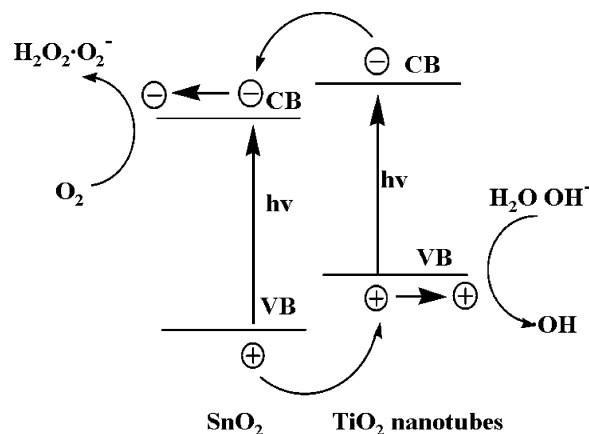


Fig. 8. Schematic diagram of the charge-transfer process in the SnO<sub>2</sub>/TiO<sub>2</sub> nanotubes composite photocatalysts.

NHE at pH 7) loaded on the surface of TiO<sub>2</sub> nanotubes. That is to say, the conduction band of SnO<sub>2</sub> acts as a sink for photogenerated electrons. While the photogenerated holes move in the opposite direction, they accumulate in the valence band of the TiO<sub>2</sub> nanotubes, which increases the efficiency of charge separation [16,17].

#### 4. Conclusions

TiO<sub>2</sub> nanotubes have been prepared in the hydrothermal condition. Further through loading SnO<sub>2</sub> on them by solvothermal process, we have successfully synthesized the SnO<sub>2</sub>/TiO<sub>2</sub> nanotubes composite photocatalysts. MB being the target pollutant, we have systemically investigated the photocatalytic performance. The results demonstrated that the composite photocatalyst with proper amount of SnO<sub>2</sub> loading owns better photocatalytic activity than the pure TiO<sub>2</sub> nanotubes. The composite photocatalysts can not only make MB at a high concentration level around the surface of the composite photocatalysts by their strong adsorption properties but also decrease the recombination rate of electron–hole pairs so as to achieve good photocatalytic performance. Moreover, the effect of SnO<sub>2</sub> contents on the photocatalytic activity was also investigated. It was found that the best photocatalytic activity was obtained in the case of 5 wt.% SnO<sub>2</sub> loading.

#### Acknowledgement

This work was supported by National Natural Science Foundation of China (No. 20403014) and Key Project of Chinese MOE.

#### References

- [1] M.R. Hoffmann, S.T. Martin, W. Choi, D.W. Bahnemann, Environmental applications of semiconductor photocatalysis, *Chem. Rev.* 95 (1995) 69–96.
- [2] M.A. Fox, M.T. Dulay, Heterogeneous photocatalysis, *Chem. Rev.* 93 (1993) 341–357.
- [3] A.L. Linsebigler, G. Lu, J.T. Yates, Photocatalysis on TiO<sub>2</sub> surfaces: principles, mechanisms, and selected results, *Chem. Rev.* 95 (1995) 735–758.
- [4] T.Y. Zhang, T. Oyama, A. Aoshima, H. Hidaka, J.C. Zhao, N. Serpone, Photooxidative *N*-demethylation of methylene blue in aqueous TiO<sub>2</sub> dis-

- persions under UV irradiation, *J. Photochem. Photobiol. A: Chem.* 140 (2001) 163–172.
- [5] M.W. Xu, S.J. Bao, X.G. Zhang, Enhanced photocatalytic activity of magnetic TiO<sub>2</sub> photocatalyst by silver deposition, *Mater. Lett.* 59 (2005) 2194–2198.
- [6] D. Chatterjee, A. Mahata, Visible light induced photodegradation of organic pollutants on dye adsorbed TiO<sub>2</sub> surface, *J. Photochem. Photobiol. A: Chem.* 153 (2002) 199–204.
- [7] H. Tada, Y. Kubo, M. Akazawa, S. Iro, Promoting effect of SiO<sub>x</sub> monolayer coverage of TiO<sub>2</sub> on the photoinduced oxidation of cationic surfactants, *Langmuir* 14 (1998) 2936–2939.
- [8] S. Pilkenton, D. Raftery, Solid-state NMR studies of the adsorption and photooxidation of ethanol on mixed TiO<sub>2</sub>–SnO<sub>2</sub> photocatalysts, *Solid State Nucl. Mag.* 24 (2003) 236–253.
- [9] P.V. Kamat, K. Vinodgopal, Environmental photochemistry with semiconductor nanoparticles, in: V. Ramamurthy, K.S. Schanze (Eds.), *Organic and Inorganic Photochemistry*, Marcel Dekker, New York, 1998.
- [10] C.H. Kwon, H. Shin, J.H. Kim, W.S. Choi, K.H. Yoon, Degradation of methylene blue via photocatalysis of titanium dioxide, *Mater. Chem. Phys.* 86 (2004) 78–82.
- [11] J.C. Xu, M. Lu, X.Y. Guo, H.L. Li, Zinc ions surface-doped titanium dioxide nanotubes and its photocatalysis activity for degradation of methyl orange in water, *J. Mol. Catal. A: Chem.* 226 (2005) 123–127.
- [12] M. Hodos, E. Horváth, H. Haspel, Á. Kukovecz, Z. Kónya, I. Kiricsi, Photosensitization of ion-exchangeable titanate nanotubes by CdS nanoparticles, *Chem. Phys. Lett.* 399 (2004) 512–515.
- [13] Y.J. Lin, L. Wang, W.Y. Chiu, Preparation and characterization of titania nanotubes and hybrid materials derived from them, *J. Vac. Sci. Technol. B* 23 (2005) 2398–2402.
- [14] C. Wang, X.M. Wang, B.Q. Xu, J.C. Zhao, B.X. Mai, P.A. Peng, G.Y. Sheng, J.M. Fu, Enhanced photocatalytic performance of nanosized coupled ZnO/SnO<sub>2</sub> photocatalysts for methyl orange degradation, *J. Photochem. Photobiol. A: Chem.* 168 (2004) 47–52.
- [15] C. Wang, J.C. Zhao, X.M. Wang, B.X. Mai, G.Y. Sheng, P.A. Peng, J.M. Fu, Preparation, characterization and photocatalytic activity of nano-sized ZnO/SnO<sub>2</sub> coupled photocatalysts, *Appl. Catal. B: Environ.* 39 (2002) 269–279.
- [16] L.Y. Shi, C.Z. Li, H.C. Gu, D.Y. Fang, Morphology and properties of ultra-fine SnO<sub>2</sub>–TiO<sub>2</sub> coupled semiconductor particles, *Mater. Chem. Phys.* 62 (2000) 62–67.
- [17] Y.M. Cui, S.H. Fan, Synthesis, characterization and application of complex nanometer particles of Rh<sup>3+</sup>/TiO<sub>2</sub>/SnO<sub>2</sub> in photocatalytic degradation of particles, *Chin. Photograph. Sci. Photochem.* 21 (2003) 161.